International Journal of Nanomedicine Dovepress

Open Access Full Text Article ORIGINAL RESEARCH

Extracellular Vesicles Derived from Lipopolysaccharide-Pretreated Periodontal Ligament Stem Cells Ameliorate Inflammatory Responses in Experimental Colitis via the PI3K/AKT Signaling Pathway

Shuai Tang[1–4], Wenyu Feng[2–4], Zekun Li[1], Xinjuan Liu[1], Tong Yang[1–4], Fulan Wei[2–4], Gang Ding[1]

[1]School of Stomatology, Shandong Second Medical University, Weifang, Shandong, 261053, People's Republic of China; [2]Department of Orthodontics, School and Hospital of Stomatology, Cheeloo College of Medicine, Shandong University, Jinan, Shandong, 250012, People's Republic of China; [3]Shandong Key Laboratory of Oral Tissue Regeneration, Shandong University, Jinan, Shandong, 250012, People's Republic of China; [4]Shandong Provincial Clinical Research Center for Oral Diseases, Shandong University, Jinan, Shandong, 250012, People's Republic of China

Correspondence: Gang Ding, School of Stomatology, Shandong Second Medical University, Baotong West Street No. 7166, Weifang, Shandong, 261053, People's Republic of China, Email dinggang@sdsmu.edu.cn; Fulan Wei, Department of Orthodontics, School and Hospital of Stomatology, Cheeloo College of Medicine, Shandong University, Wenhua West Road No. 44-1, Jinan, Shandong, 250012, People's Republic of China, Email weifl@sdu.edu.cn

Introduction: Inflammatory bowel disease is a complex chronic inflammatory condition characterized by dysbiosis of the gut microbiota and dysregulation of immune system. In recent years, extracellular vesicles (EVs) derived from mesenchymal stem cells have garnered significant attention for their beneficial potentials in immune modulation and tissue repair. This study aims to evaluate the therapeutic effects and underlying mechanisms of EVs derived from lipopolysaccharide (LPS)-pretreated periodontal ligament stem cells (PDLSCs) in mice with colitis.

Methods: A mouse model of colitis was established using 3.0% dextran sulfate sodium (DSS). Following the induction of colitis, mice were treated via tail vein injection with either conventional PDLSC-derived EVs (P-EVs) or LPS-pretreated PDLSC-derived EVs (LPS pre-EVs). The EVs were characterized using transmission electron microscopy, nanoparticle tracking analysis, and Western blot analysis. The therapeutic effects and mechanisms were evaluated through a combination of small animal live imaging, disease activity index (DAI) scoring, histopathological staining, qRT-PCR, 16S rRNA gene sequencing, and mass spectrometry analysis.

Results: The LPS pre-EVs exhibited typical EVs characteristics in terms of morphology, particle size distribution, and marker protein expression. Compared to P-EVs, LPS pre-EVs significantly ameliorated weight loss, DAI scores, colon length, and perianal symptoms in DSS-induced murine colitis. Additionally, LPS pre-EVs up-regulated the expression of Arginase-1, a typical M2 macrophage marker, and tight junction proteins, including ZO-1, Occludin, and Claudin-1, enhanced gut microbial diversity, and significantly regulated intestinal protein expression and activation of the PI3K/AKT signaling pathway.

Conclusion: LPS pre-EVs exhibit significant anti-inflammatory and tissue repair effects in a mouse model of colitis. The underlying mechanisms may involve the regulation of macrophage polarization, maintenance of intestinal barrier function, modulation of the gut microbiota, and activation of the PI3K/AKT signaling pathway.

Keywords: inflammatory bowel disease, periodontal ligament stem cells, extracellular vesicles, gut microbiota, PI3K/AKT signaling pathway

Introduction

Inflammatory bowel disease (IBD) is a chronic, recurrent, immune-mediated inflammatory condition of the intestine, primarily manifesting in two forms: Crohn's disease and ulcerative colitis, which often affect the ileum, rectum, and

Received: 12 September 2024
Accepted: 8 November 2024
Published: 18 November 2024

Graphical Abstract

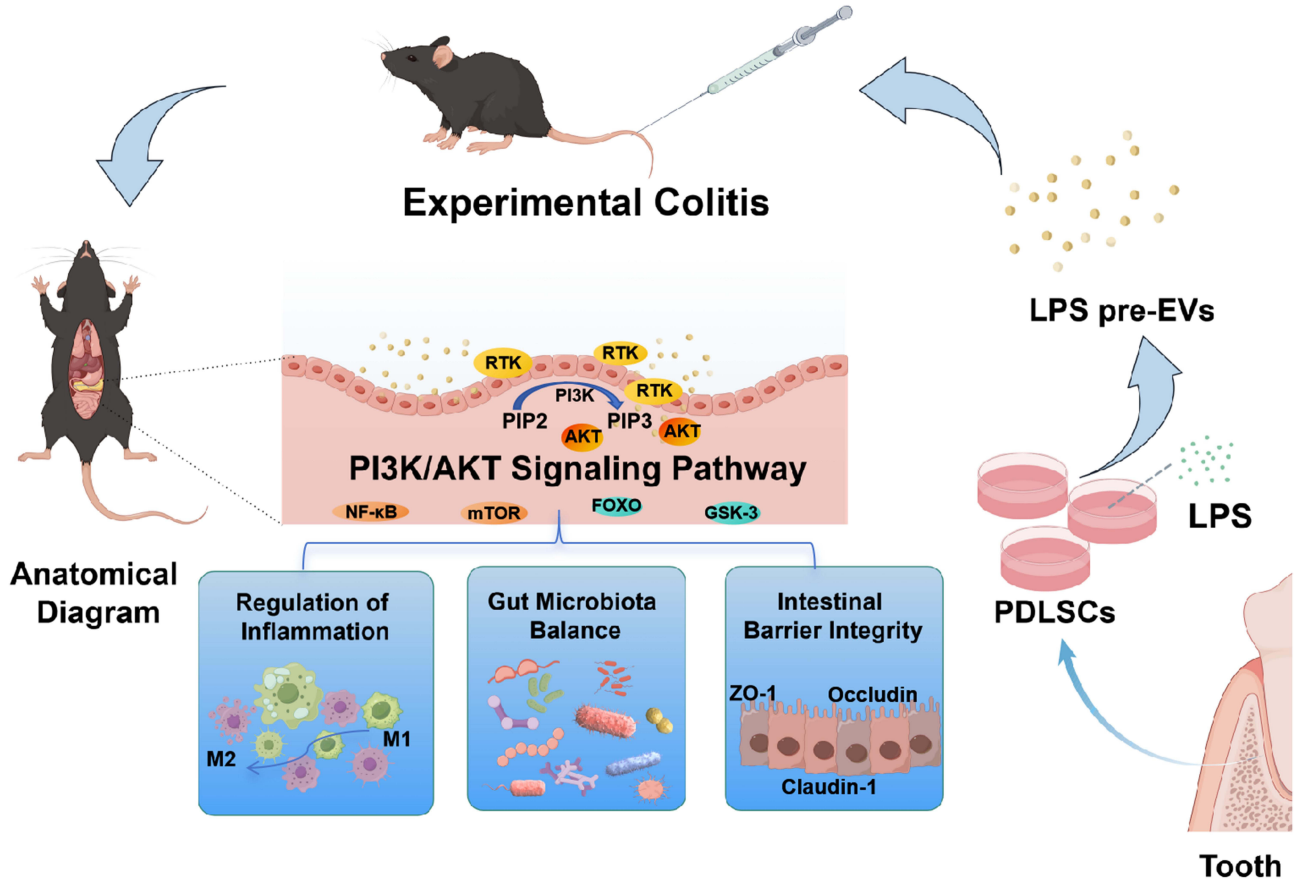

colon, leading to chronic inflammation and ulcer formation within the gastrointestinal tract. As a result, IBD patients experience symptoms such as weight loss, abdominal pain, diarrhea, and other gastrointestinal issues.[1,2] The pathogenesis of IBD remains unclear, but it is widely believed to involve multiple factors, including the immune responses, genetic predisposition, environmental influences, and the impact of gut microbiota on the body.[3,4] In patients with IBD, profound microenvironmental changes typically occur at the sites of intestinal mucosa. These changes include local nutrient depletion, an imbalance between oxygen supply and demand in the tissue, and the production of reactive nitrogen and oxygen intermediates.[5,6] The resulting oxidative stress, endoplasmic reticulum stress, and hypoxic stress signaling affect several key features, such as the integrity of the intestinal mucosal barrier, the survival of intestinal cells, immune regulation, and the diversity of the gut microbiota.[4] In the IBD microenvironment, cytokine-mediated interactions between immune cells and other cell types are complex and dynamic, contributing to the worsening severity of the disease. A variety of immune cells, such as polymorphonuclear neutrophils, macrophages, and monocytes, along with adaptive immune cells like T cells and B cells, are recruited to sites of active inflammation in response to chemokine signals produced there, including interleukin (IL)-8, leukotriene B4, platelet-activating factor, complement factor C5a, and N-formylated peptides.[7] The incidence of IBD is gradually increasing and affecting younger populations, which has drawn widespread attention internationally.[8–10] Researchers are dedicated to gaining a deeper understanding of the pathogenesis, biomarkers, diagnostic methods, and personalized treatment strategies for IBD. The primary goal of IBD treatment is to correct immune dysregulation and suppress intestinal mucosal inflammation, with current therapies relying mainly on anti-inflammatory drugs, immunomodulators, thiopurines, and monoclonal antibodies. However, the

effectiveness of these treatments remains suboptimal.[11–13] Therefore, there is an urgent need to explore new therapeutic approaches for IBD.

In recent years, cell therapy has shown promising effects in the treatment of IBD.[14,15] Mesenchymal stem cells (MSCs), a type of multipotent stem cell derived from postnatal tissues, possess various biological functions, including immune modulation, promotion of tissue repair and regeneration, and intercellular communication and regulation.[16–20] A growing body of studies indicated that the release of extracellular vesicles (EVs) is a key pathway through which MSCs exert their biological effects. As small membrane-bound structures formed by the inward budding of intraluminal vesicles within multivesicular endosomes, the EVs carry a variety of bioactive molecules, such as proteins, RNA, and DNA.[21–23] Given the significant regulatory roles of MSCs and their EVs in various diseases, it is crucial to further explore their specific therapeutic effects on IBD, as well as the possible mechanisms.[24–26]

Periodontal ligament stem cells (PDLSCs) are specific adult stem cells isolated from the periodontal ligament of teeth and exhibit characteristics similar to MSCs.[27,28] Compared to other MSCs, PDLSCs have advantages such as ease of collection, strong colony-forming ability, and substantial cellular reserves.[29,30] In addition, it was shown that when MSCs are co-cultured with inflammatory cytokines or inflammatory small-molecule chemicals, their abilities of migration to injury sites, exertion of paracrine effects, and regulation of immune system are significantly enhanced.[31–34] Lipopolysaccharide (LPS), a endotoxin found in the outer membrane of Gram-negative bacteria, could activate immune-related cells, and stimulate them to produce and secrete inflammatory factors, thereby playing a crucial role in the immune system.[35,36]

In this study, the EVs of LPS-pretreated PDLSCs (LPS pre-EVs) were collected and characterized, and used to explore their therapeutic effects on IBD. Moreover, the underlying mechanisms were also investigated. The results demonstrated that LPS pre-EVs may offer unique efficacious outcome in IBD, thus providing new options and ideas for treating this disease.

Materials and Methods

The study involving human samples has received ethical approval from the Ethics Committee of Shandong Second Medical University (Approval No. 2021YX090) and complied with the Declaration of Helsinki. All animal experiments in this study were approved by the Ethics Committee of the School of Stomatology, Shandong University (Approval No. 20220708). The study was conducted in strict accordance with the Animal Management Rules of the Ministry of Health of the People's Republic of China.

PDLSCs Culture and Extracellular Vesicle Extraction

Periodontal ligament tissues were obtained from healthy teeth without caries and periodontitis of patients extracted their third molars. The patients were 20–23 years old, and gave their informed consent. The tissues were washed with phosphate-buffered saline (PBS; Biosharp, Hefei, China) containing 2% antibiotics, and then separated and cultured in small periodontal ligament tissue explants. Culture medium containing α-MEM (BasalMedia, Shanghai, China), 20% fetal bovine serum (FBS; Gibco, Carlsbad, USA), 1% penicillin/streptomycin was added to the culture flasks (NEST Biotechnology, Wuxi, China), and were then placed in an incubator at 37°C in 5% CO_2. After 4 hours, the medium was replaced to initiate primary cell culture. Once the cells had expanded to a sufficient quantity, well-growing P2 to P6 PDLSCs were selected. When the cells reached approximately 60% confluence, the medium was replaced with either fresh culture medium or medium containing LPS (1 μg/mL; Solarbio, Beijing, China). After 24 hours, when the cells had reached 70% to 80% confluence, the medium was replaced with culture medium containing 5% EVs-free FBS (LONSERA, Suzhou Shuangru. China). The cells were then cultured for an additional 48 hours, after which the cell culture supernatant was collected, centrifuged to remove cells and debris, and stored at −80°C. Once a sufficient amount of cell culture supernatant has been collected, EVs are extracted (Figure 1A).

Identification of EVs

Transmission Electron Microscopy (TEM) Analysis: The extracted EVs were diluted to a concentration of 10–100 μg/mL. A 20 μL drop of the EV suspension was placed onto a carbon-coated copper grid and allowed to stand for 5–10 minutes. The

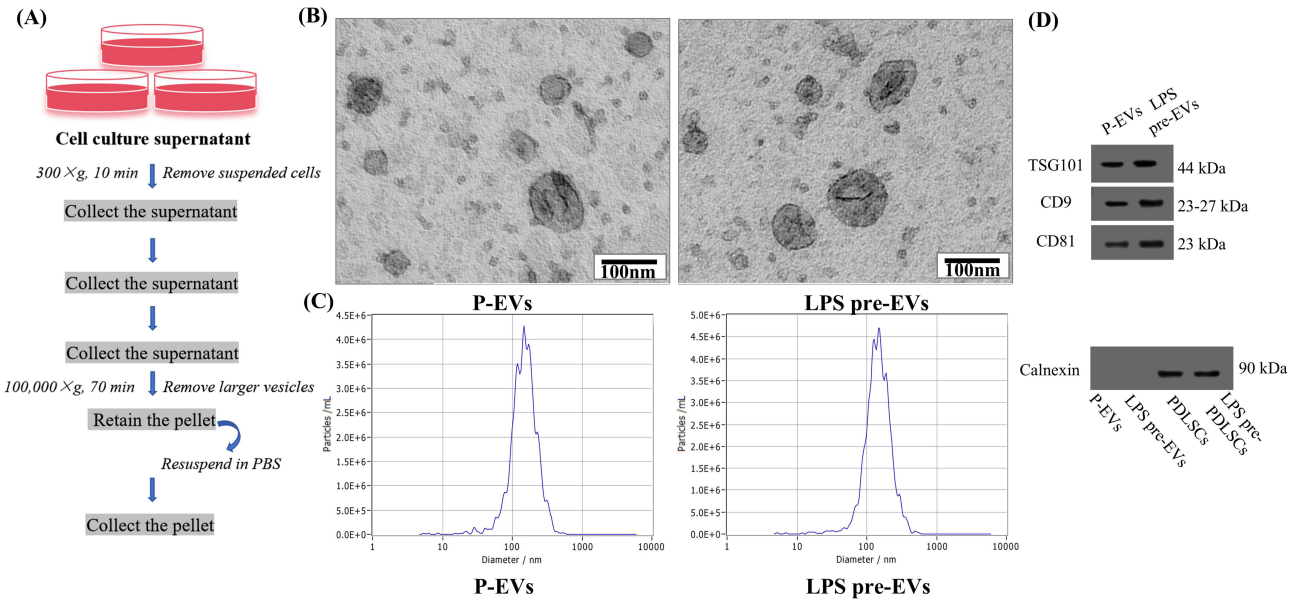

Figure 1 Extraction and characterization of EVs (**A**) The workflow for the extraction of EVs. **(B)** Transmission electron microscopy images: P-EVs and LPS pre-EVs exhibit typical vesicular structures. Scale bars: 100 nm. **(C)** Nanoparticle tracking analysis: the size distribution of P-EVs and LPS pre-EVs is primarily concentrated between 100–200 nm. **(D)** Western blot analysis: both P-EVs and LPS pre-EVs were positive for TSG101, CD9, and CD81, while Calnexin is expressed only in PDLSCs and LPS pre-PDLSCs.

grid was then rinsed with distilled water to remove any unabsorbed sample. Afterwards, the grid was stained with 2% phosphotungstic acid for 1 minute and allowed to dry in the air. After 20 minutes, the dried copper grid was placed on a sample holder and observed under a TEM, where the morphology of the EVs was visualized and recorded.

Particle Size Analysis: The extracted EVs were diluted to a concentration of 10^7-10^9 particles/mL. The sample was then loaded into a calibrated nanoparticle tracking analyzer. After ensuring that there were no air bubbles in the sample chamber, particle size analysis was conducted. The size distribution and concentration data of the EVs were obtained and presented in the form of a size distribution curve, with the peak representing the average particle size of the EVs.

Western Blot: The extracted EVs were analyzed for the expression of specific markers (Abcam, Cambridge, UK), including TSG101, CD81, CD9, and Calnexin, using the Western blot procedure as described later in the text.

Animal Model Establishment and Treatment

Female C57BL/6 mice (Pengyue, Jinan, China), aged 7 weeks and weighing between 18–20 g, were housed in the animal laboratory. The mice were acclimatized to the environment and diet for one week. All mice were in a healthy state and were randomly divided into four groups, with six mice in each group: the normal control group (Control), dextran sulfate sodium (DSS)-induced experimental colitis model group (DSS), PDLSC-derived EVs treatment group (P-EVs), and LPS-pretreated PDLSC-derived EVs treatment group (LPS pre-EVs).

Preliminary experiments determined that a 3% concentration of DSS was appropriate to meet the experimental requirements. The appropriate amount of DSS powder was weighed and fully dissolved in autoclaved purified water. Before starting the experiment, mice were fasted and deprived of water for approximately 4 hours. The Control group was provided with autoclaved purified water, while the DSS, P-EVs, and LPS pre-EVs groups were provided with 3% DSS solution. The DSS solution or autoclaved purified water was refreshed every 2–3 days. On days 1, 3, and 5, the Control and DSS groups were injected with 200 μL of PBS via tail vein injection, while the P-EVs group and LPS pre-EVs group were injected with 200 μL of P-EVs and LPS pre-EVs, respectively. Body weight, stool consistency, and the presence of fecal blood were monitored daily at the same time. On day 7, all mice were euthanized. During this period, the disease activity index (DAI) of the mice was assessed, the overall condition of the colon and spleen was observed, and serum and tissue samples were collected for subsequent analysis.

Animal Live Imaging Analysis

According to the reagent instructions, DIR dye working solution (Umibio, Shanghai, China) was prepared and used to label the extracted EVs, resulting in P-EVs-DIR and LPS pre-EVs-DIR complexes. These labeled complexes were then administered via tail vein injection to the mice in the P-EVs and LPS pre-EVs groups, respectively. After 12 hours, the mice were placed in a small animal in vivo imaging system to observe and record the fluorescence intensity and distribution within organs such as the colon and spleen.

Colonic Histological Examination

Approximately 1 cm segments of colon tissue were cut and placed into labeled embedding cassettes, followed by fixation in 4% paraformaldehyde for 24 hours. After fixation, the tissues were washed with water and dehydrated using a semi-automatic benchtop tissue processor. The tissues were then cleared and embedded in paraffin. Subsequently, the embedded tissues were trimmed and sectioned using a microtome. The sections were stored at room temperature until needed for staining. The sections were de-paraffinized and stained according to the specific requirements of the experiment, including HE staining, Alcian Blue staining, immunohistochemical staining, and immunofluorescence staining, following the instructions provided in the reagent kits. After staining, the slides were examined under a microscope at various magnifications, and images were captured for further analysis.

Western Blot Analysis

The samples were lysed in protein lysis buffer. Then 5× SDS-PAGE loading buffer was added to the samples, and they were heated in a metal bath at 100°C for 5–10 minutes to denature the proteins. The samples were then cooled and stored at −20°C until further use. An appropriate amount of each sample was used for Western blot analysis. The separation and stacking gels were prepared according to standard procedures. The protein samples, along with a molecular weight marker (EC0019, Shandong Sparkjade Biotechnology Co., Ltd., China), were loaded into the wells of the gel. SDS-PAGE was performed to separate the proteins, which were then transferred onto a PVDF membrane. After the transfer, the membrane was blocked with TBST blocking buffer and incubated with the primary antibodies overnight. The next day, the membrane was washed and then incubated with the secondary antibody. After washing, the membrane was treated with enhanced chemiluminescence detection reagent for visualization. The results were detected and the band images were captured and saved using a fluorescence imaging system.

RNA Isolation and qRT-PCR

The collected colon tissue samples were removed from liquid nitrogen and ground into a paste in a mortar. The ground tissue samples were then mixed with an appropriate amount of Trizol lysis buffer. RNA extraction and precipitation were carried out according to the instructions provided in the RNA extraction kit (AG, Accurate biotechnology, Changsha, China). The concentration and purity of the RNA were measured using a Nanodrop spectrophotometer. The instrument was first cleaned and calibrated with 1 μL of DEPC water, followed by the measurement of 1 μL of RNA sample to ensure the RNA quality met the requirements for subsequent experiments. The total RNA was reverse transcribed to generate cDNA using Evo M-MLV RT Kit with gDNA Clean for qPCR (AG) and qRT-PCR was performed with the Evo M-MLV One Step RT-qPCR Kit (SYBR) (AG) on a Roche LightCycler® 480II (Roche Diagnostics GmbH, Mannheim, Germany) under standard cycling conditions: 42°C for 5min, 95°C for 10s, 40 cycles of 95°C for 5 s, 60°C for 30s. Gene expression levels were quantified using the $2^{-\Delta\Delta CT}$ method. Primer sequences are detailed in Table 1.

Fecal Microbiome Sequencing and Colonic Proteomics Analysis

Fecal Microbiome Sequencing: The 16S rRNA gene sequencing method was used to extract microbial genomic DNA from mouse fecal samples. The quality of the DNA was assessed using 0.8% agarose gel electrophoresis. Specific primers targeting the conserved regions of the V3-V4 region were used to amplify the DNA. The amplified products were then purified and subjected to fluorescence quantification to prepare the sequencing library. After quality control, the library was sequenced by a specialized company. Data analysis involved quality control using Trimmomatic (v 0.39) and

Table 1 Primer sequences

Primer name	Primer sequences
IL-10	FOR: AAGTCCGGAGAGGAGACTTC
	REV: TGGATGGTCTTGGTCCTTAG
IL-6	FOR: AAGTCCGGAGAGGAGACTTC
	REV: TGGATGGTCTTGGTCCTTAG
TNF-α	FOR: AACTCCAGGCGGTGCCTATG
	REV: TCCAGCTGCTCCTCCACTTG
β-actin	FOR: CTCAGGAGGAGCAATGATCT
	REV: GACCTGTACGCCAACACAGT

Note: IL-10: Interleukin-10, IL-6: Interleukin-6, TNF-α: Tumor Necrosis Factor-alpha.

merging of paired-end sequences using FLASH (v 1.2.11). Operational Taxonomic Unit clustering was performed at 85% similarity using the QIIME2 pipeline and Closed-reference clustering method. Functional prediction analysis was conducted using PICRUSt with KEGG pathway analysis.

Colonic Proteomics Analysis: Proteins were extracted from colonic tissue samples using a lysis buffer containing 8 M urea and protease inhibitors. The protein concentration was measured, followed by treatment with dithiothreitol and iodoacetamide for reduction and alkylation, respectively. Samples were then digested using the FASP (Filter-Aided Sample Preparation) method, and desalting was performed using ultrafiltration and C18 desalting columns. The samples were subjected to DIA (Data-Independent Acquisition) mass spectrometry analysis by a professional service provider. The Uniprot mouse database was used for database searching, and the results were evaluated at both the peptide and protein levels for qualitative and quantitative protein analysis.

Image and Statistical Analysis

All data are presented as mean ± SEM. Statistical analysis was performed using GraphPad Prism 9.0 (GraphPad Software, La Jolla, CA, United States), with ANOVA used to assess differences between groups. The quantitative analysis was performed using ImageJ software. A value of $P < 0.05$ was considered statistically significant.

Results

LPS Pre-EVs Exhibited Typical Characteristics of EVs

Both P-EVs and LPS pre-EVs exhibited typical extracellular vesicle morphology, presenting as round, oval, and horseshoe-shaped vesicular structures with intact membrane integrity (Figure 1B). The size distribution of EVs in both groups was concentrated between 100–200 nm, with the peak size for P-EVs at 148 nm and for LPS pre-EVs at 149 nm, showing no significant difference in size distribution between the two groups (Figure 1C). Western blot analysis further confirmed the expression of EVs markers, demonstrating that the markers TSG101, CD9, and CD81 were expressed in both P-EVs and LPS pre-EVs, while the endoplasmic reticulum protein Calnexin was not detected in the EVs samples but was present in PDLSC cell lysates (Figure 1D). These results indicate that the extracted EVs samples were of high purity and exhibited typical EVs characteristics, confirming the successful isolation of standard EVs for subsequent research.

LPS Pre-EVs Demonstrated Significant Anti-Inflammatory Therapeutic Effects in Mice with Colitis

The experimental workflow of this study is illustrated in Figure 2A. In the mouse colitis model experiment, the Control group exhibited normal fecal morphology, with feces appearing as pellets or elongated forms in dark brown or brown color. Mice in the P-EVs and LPS pre-EVs groups showed higher moisture content in their feces, which appeared on the second day. By the fourth day bloody stools were in the mice of the P-EVs and LPS pre-EVs groups, whose

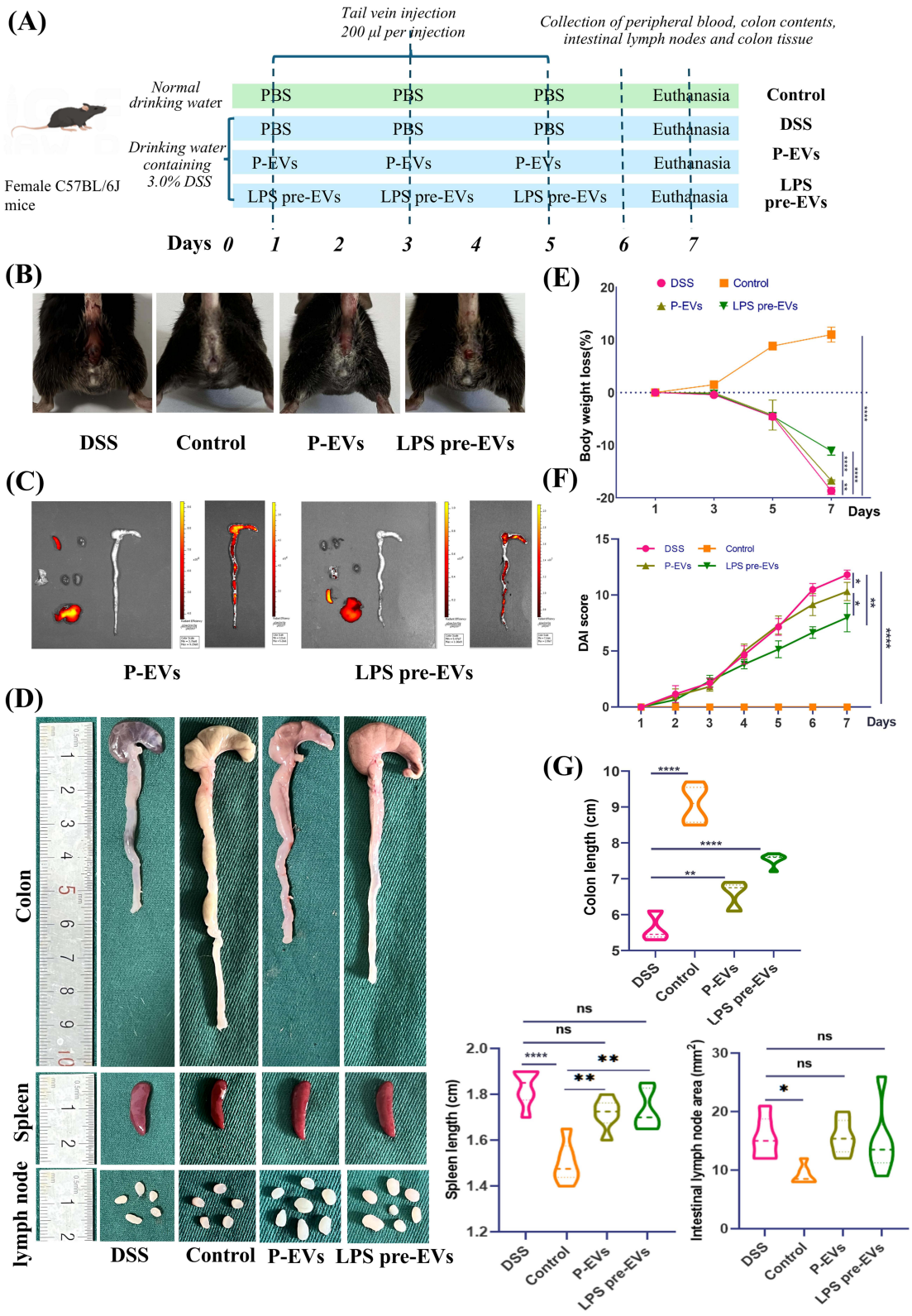

Figure 2 Protective effects of LPS pre-EVs on DSS-induced colitis in mice **(A)** Schematic of the animal experiment design. **(B)** Perianal condition of mice. **(C)** In vivo imaging showing accumulation of labeled EVs in the colon, with stronger fluorescence in the LPS pre-EVs group. **(D)** Macroscopic images of the colon, spleen, and mesenteric lymph nodes: better recovery of colon length in the LPS pre-EVs group, with minimal changes in the spleen and lymph nodes. **(E)** Body weight changes, with the least weight loss observed in the LPS pre-EVs group. **(F)** DAI scores. **(G)** Statistical analysis of colon length, spleen length, and lymph node area. *P < 0.05, **P < 0.01, ****P < 0.0001, ns: not significant.

symptoms were milder than that in DSS group usually exhibiting bloody stools earlier. Upon euthanasia on the seventh day, the mice in Control group had clean perianal areas (Figure 2B).

Small animal live imaging results (Figure 2C) indicated that the labeled EVs primarily accumulated in the colonic region, with the LPS pre-EVs group showing stronger fluorescence signals. After euthanizing the mice, the colon and rectum tissues were collected, and the length was measured using the terminal end of the cecum as a reference point (Figure 2D). The results showed that the Control group had the longest colon and rectum lengths, while the DSS group exhibited a significant reduction in colon length, confirming the successful establishment of the IBD model. Treatment with P-EVs and LPS pre-EVs led to a partial recovery in colon length, with the LPS pre-EVs group showing the most pronounced recovery. The mice in the Control group showed a gradual weight increase over time, while those in the DSS, P-EVs, and LPS pre-EVs groups began to lose weight starting on day 3. Between days 5 and 7, the DSS and P-EVs groups exhibited significant weight loss, with reductions of 14.16% and 10.60%, respectively. In contrast, the LPS pre-EVs group experienced a smaller decrease in body weight, with a reduction of 6.65% (Figure 2E). DAI scores were assessed across all groups. In the 1–3 days, no significant changes in DAI were observed in the DSS, P-EVs, and LPS pre-EVs groups. However, the DSS group showed a sharp increase in DAI on day 5, which continued to rise. The P-EVs group exhibited an increase in DAI starting on day 3, but the subsequent rise slowed down. The DAI of LPS pre-EVs group increases more slowly than that of P-EVs group after day 3 (Figure 2F). Measurements of the spleen and mesenteric lymph nodes (Figure 2G) revealed that the spleen was significantly enlarged in the DSS, P-EVs, and LPS pre-EVs groups compared to the Control group. However, there were no significant differences in spleen length and mesenteric lymph node diameter among the treated groups.

In the HE staining (Figure 3A), the DSS group showed significant damage to the intestinal wall, accompanied by marked infiltration of inflammatory cells. After treatment with P-EVs and LPS pre-EVs, the intestinal wall damage in the IBD model mice was improved, and the infiltration of inflammatory cells was alleviated. In the Alcian blue staining (Figure 3B), the DSS group exhibited severe disruption of the extracellular structure of the intestinal mucosa, while the damage to the intestinal cell structure was notably reduced in the LPS pre-EVs treated group. In summary, LPS pre-EVs significantly alleviated DSS-induced IBD symptoms in mice, as evidenced by reduced weight loss, lower DAI scores, restored colon length, and improved perianal symptoms, demonstrating strong therapeutic potential.

LPS pre-EVs Modulated Intestinal Macrophage Polarization, Maintained Intestinal Epithelial Barrier Function, and Improved Inflammatory Status

Immunohistochemical staining (Figure 4A) and Western blot analysis (Figure 4B) were performed. The results showed that the expression of Arginase-1(Arg-1), a typical M2 macrophage marker, in the intestinal tissue of mice in the LPS pre-EVs group was significantly higher than that in other groups, while the expression of inducible nitric oxide synthase (iNOS), a typical M1 macrophage marker, was notably higher in the P-EVs group compared to the LPS pre-EVs group. The levels of tight junction proteins, including ZO-1, Occludin, and Claudin-1, in the intestinal epithelium were lower in the DSS group, whereas their expression was significantly enhanced in the LPS pre-EVs group (Figure 5A and B, Supplementary Figure 1-3) Additionally, qRT-PCR results (Figure 5C) indicated that, compared to the DSS group, the expression of pro-inflammatory cytokines IL-6 and TNF-α in the colonic tissue of mice in the P-EVs and LPS pre-EVs groups was significantly reduced, while the expression of the anti-inflammatory cytokine IL-10 was significantly increased.

LPS Pre-EVs Significantly Influenced the Diversity and Composition of the Gut Microbiota in Mice

Analysis of the 16S rRNA gene sequencing of fecal samples from different treatment groups (Figure 6, Supplementary Figure 4 and 5) revealed that the microbial abundance distribution in the mouse gut varied across groups, with the LPS pre-EVs group exhibiting a unique microbial community profile. *Lachnospiraceae_UCG-001* showed relatively high abundance across all groups, while *Clostridia_UCG-014* was significantly more abundant in the LPS pre-EVs group compared to other groups, suggesting that LPS pre-EVs have a regulatory effect on this microbial population. Additionally, *Streptococcus* was significantly more abundant in the DSS group than in other groups, but its abundance was markedly reduced in the LPS pre-EVs group, indicating that LPS pre-EVs treatment may suppress the overgrowth of

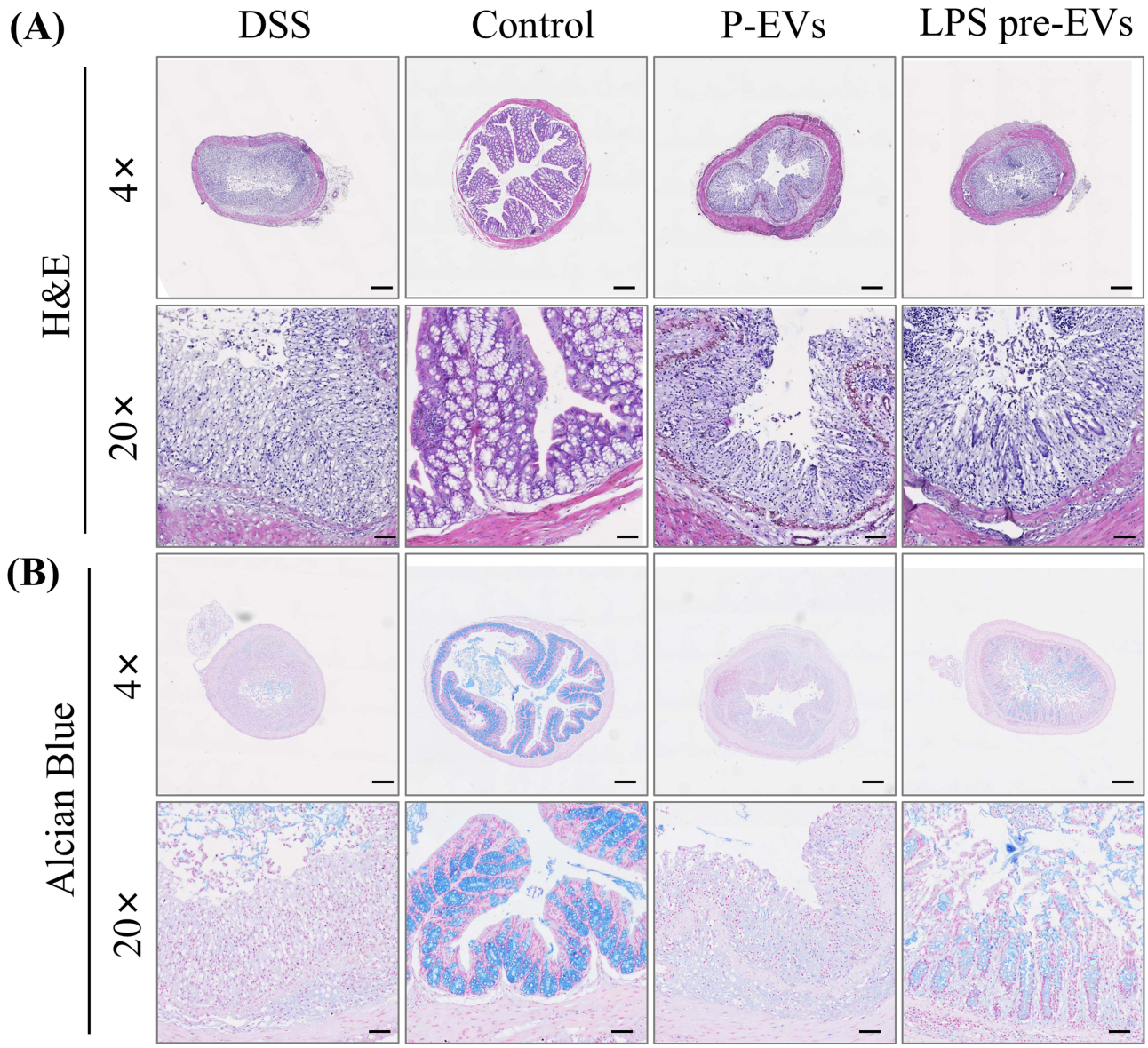

Figure 3 Histological analysis of colonic tissue in different treatment groups **(A)** H&E staining showed structural changes in colonic tissue. The DSS group exhibits severe damage and significant inflammatory cell infiltration, while the Control group shows normal structure. Both P-EVs and LPS pre-EVs groups display improved colonic integrity, with LPS pre-EVs showing more pronounced effects. **(B)** Alcian Blue staining revealed changes in the colonic mucus layer. The DSS group showed severe mucosal damage and reduced mucus, while the Control group maintains an intact mucus layer. Both P-EVs and LPS pre-EVs groups demonstrated partial restoration of mucosal structure, with LPS pre-EVs suggesting better mucus preservation than P-EVs. Scale bars: 4× =500 μm, 20× =100 μm.

certain potential pathogens. Statistical significance analysis showed that the microbial community differences between the LPS pre-EVs group and the DSS group were significant, particularly for taxa like *Aeromonas* and *Clostridia_UCG-014*, where the abundance differences reached a $P<0.01$ level. In the P-EVs group, the abundance of *Clostridia_UCG-014* significantly increased, while the abundance of *Streptococcus* significantly decreased compared to the DSS group, indicating that P-EVs may alleviate inflammation by modulating specific gut microbiota. In addition, there were differences in microbial composition between the P-EVs group and the Control group, with reduced abundance of *Shigella* and increased abundance of *Romboutsia* in the P-EVs group. These results suggest that P-EVs and LPS pre-EVs not only help suppress potential pathogens but may also promote the growth of beneficial bacteria, thereby restoring gut microbial balance. Furthermore, they can significantly alter the composition of the gut microbiota in mice, particularly in regulating gut microbiota balance, highlighting their potential therapeutic role.

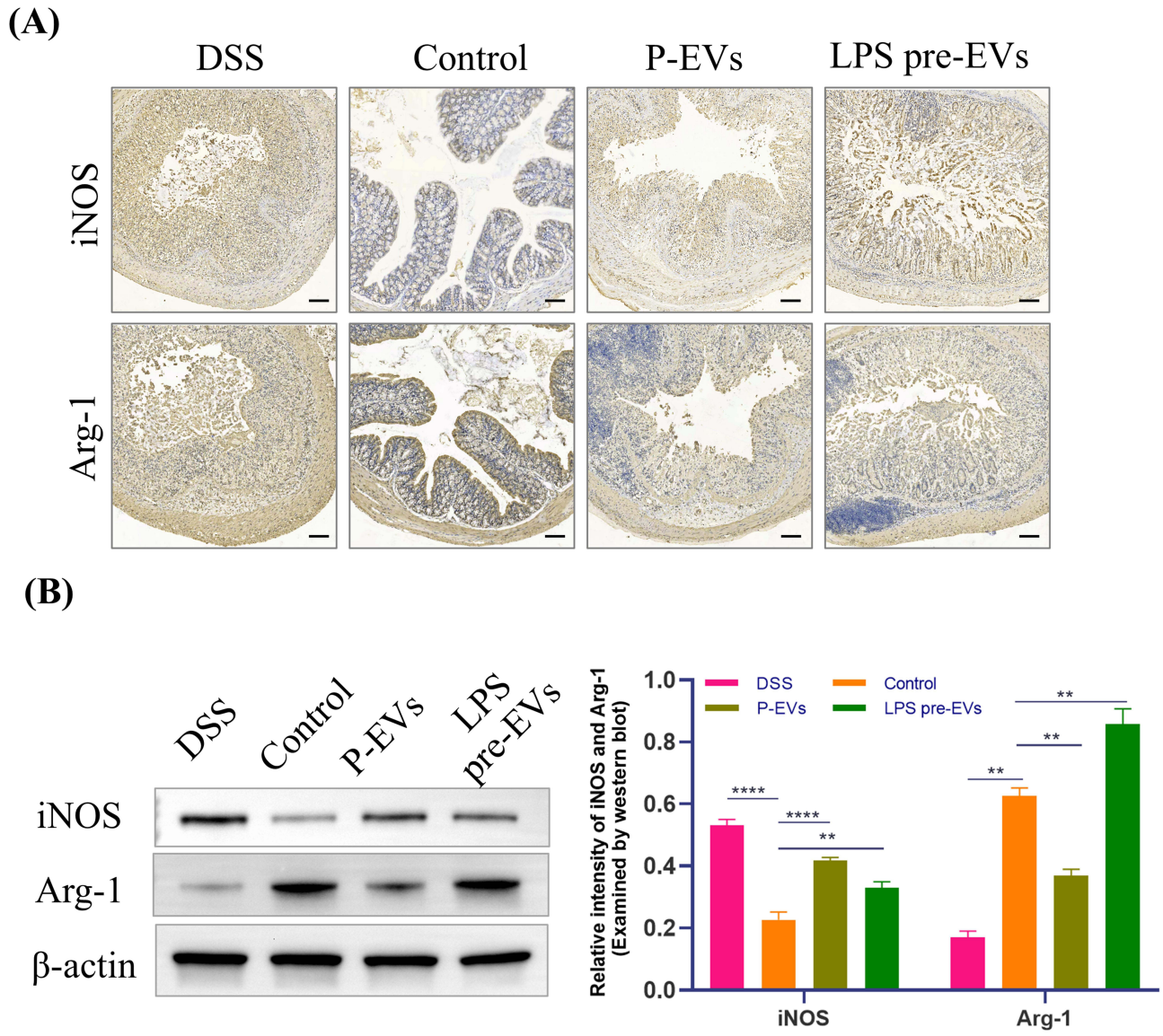

Figure 4 Effects of LPS pre-EVs on macrophage polarization **(A)** Immunohistochemical staining showed the expression of the M1 macrophage marker iNOS and the M2 macrophage marker Arg-1 in the colonic tissue of different treatment groups. The LPS pre-EVs group exhibited significantly increased Arg-1 expression, while iNOS expression was relatively lower. Scale bar: 200 μm. **(B)** Western blot analysis: iNOS expression in the LPS pre-EVs group was significantly lower than in other groups, while Arg-1 expression was significantly higher. The bar graph on the right quantifies the relative expression levels of iNOS and Arg-1 proteins. $^{**}P < 0.01$, $^{****}P < 0.0001$.

LPS pre-EVs Significantly Regulated Protein Expression in the Mouse Gut and Activated the PI3K/AKT Signaling Pathway

DIA mass spectrometry analysis revealed that LPS pre-EVs had a significant impact on protein expression in the mouse gut. The volcano plot (Figure 7A) displayed the differentially expressed proteins between the LPS pre-EVs group and the P-EVs group, with 149 proteins significantly up-regulated and 371 proteins significantly down-regulated (fold change ≥1.5, $P<0.05$). GO functional enrichment analysis of the differentially expressed proteins (Figure 7B) indicated that these proteins were primarily enriched in biological processes such as small molecule metabolic processes and single-organism metabolic processes; in cellular components, they were enriched in structures like the cytoplasm and vesicles; and in molecular functions, they were associated with oxidoreductase activity and coenzyme binding. KEGG pathway enrichment analysis (Figure 7C) further revealed that the differentially expressed proteins were significantly enriched in key metabolic and signaling pathways, including metabolic pathways, oxidative phosphorylation, glycolysis, and the complement and coagulation cascades. Cluster heatmap analysis of the differential proteins (Figure 7D) demonstrated clear

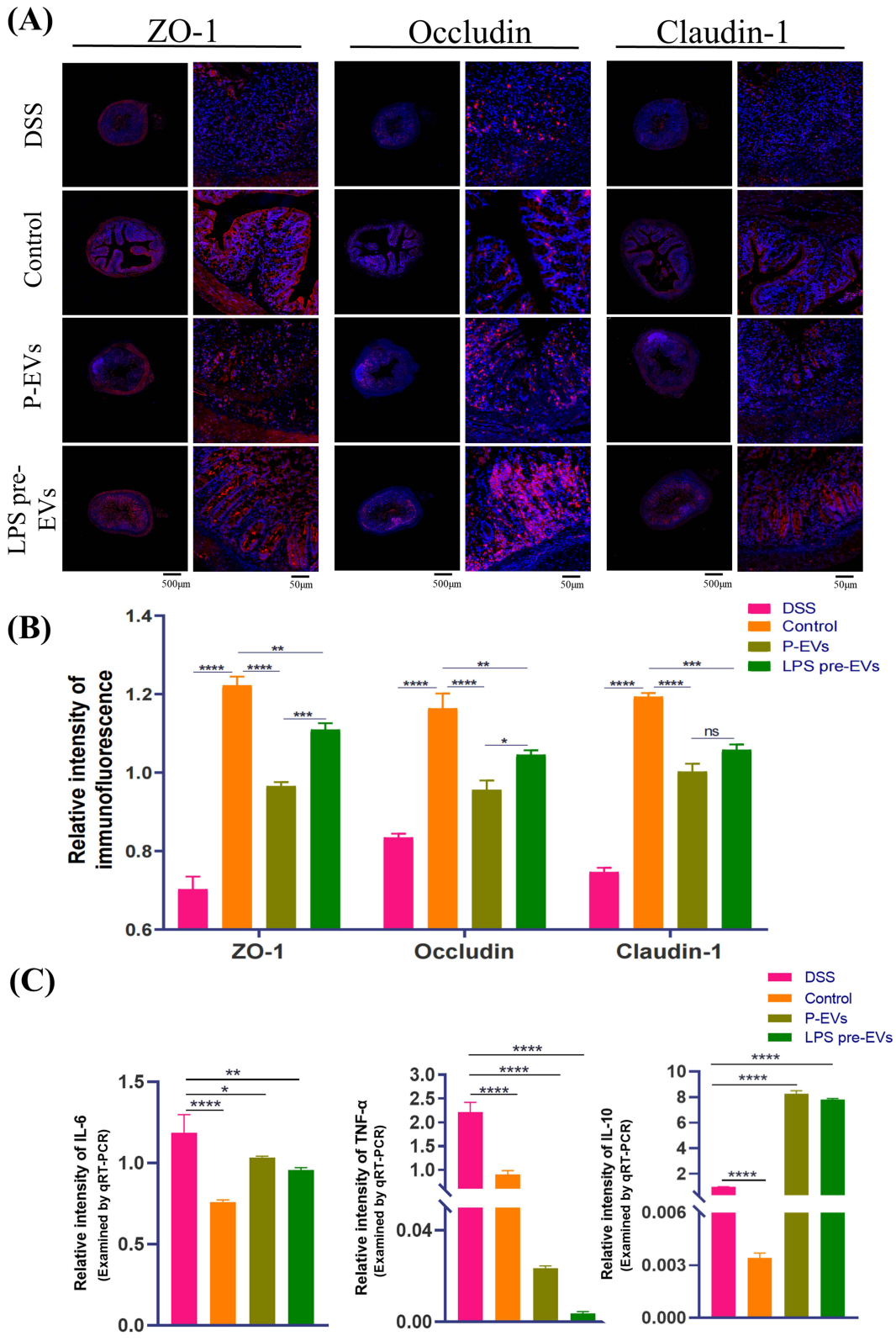

Figure 5 Effects of LPS pre-EVs on tight junction proteins and inflammatory factors in intestinal epithelium.(**A**) Immunofluorescence staining: the expression of tight junction proteins ZO-1, Occludin, and Claudin-1 in the intestinal epithelium of different treatment groups. Scale bars: 500 μm, and 50 μm, respectively. **(B)** Relative intensity of immunofluorescence. **(C)** qRT-PCR analysis: compared to the DSS group, the LPS pre-EVs group had significantly reduced expression of pro-inflammatory factors IL-6, TNF-α, while the expression of the anti-inflammatory factor IL-10 was significantly increased. P-values indicate statistical significance. **P* < 0.05, ***P* < 0.01, ****P* < 0.001, *****P* < 0.0001, ns: not significant.

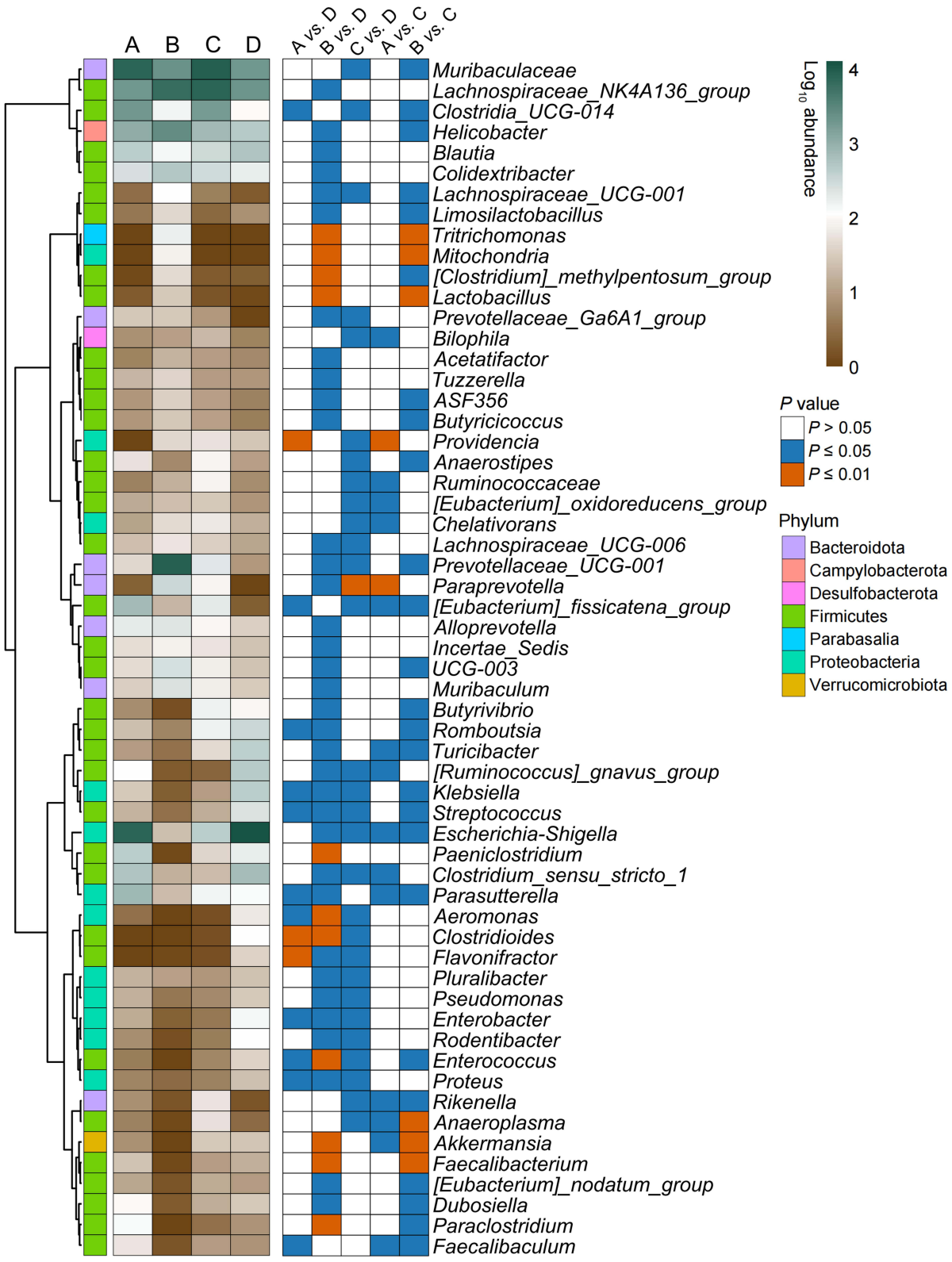

Figure 6 Regulation of gut microbiota by EVs in mice. The heatmap showed the abundance changes in gut microbiota across different treatment groups ((**A**) DSS group, (**B**) Control group, (**C**) P-EVs group, (**D**) LPS pre-EVs group). Compared to the DSS group, the P-EVs group and LPS pre-EVs group significantly increased the abundance of beneficial bacteria such as *Clostridia_UCG-014* while suppressing the overgrowth of potential pathogens like *Streptococcus* and *Aeromonas*. The P-values indicate the significance of differences between groups.

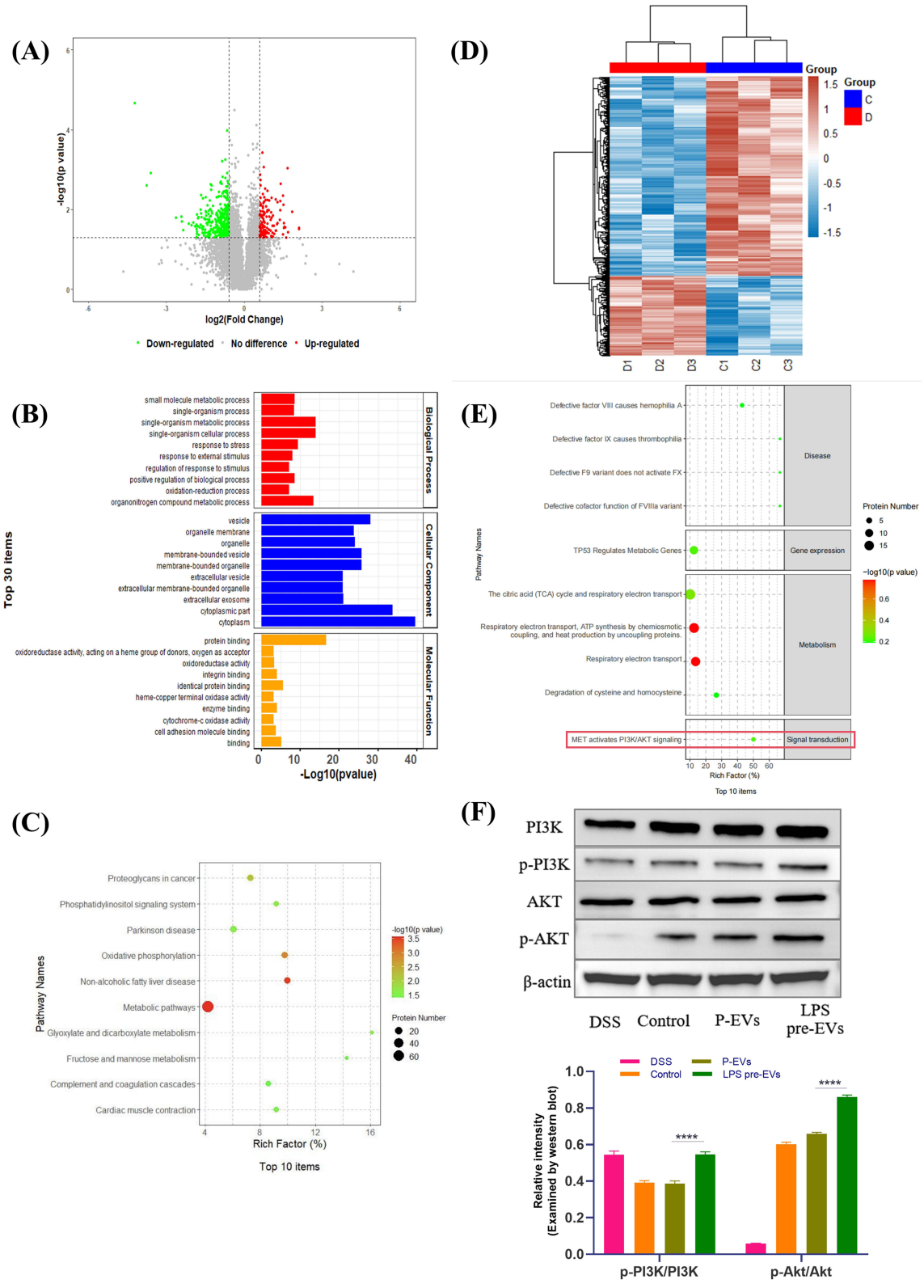

Figure 7 Effects of LPS pre-EVs on intestinal protein expression and the PI3K/AKT signaling pathway. **(A)** The volcano plot: differentially expressed proteins between the LPS pre-EVs group and the P-EVs group. **(B)** GO functional enrichment analysis. **(C)** KEGG pathway enrichment analysis. **(D)** The heatmap of differentially expressed proteins. **(E)** Reactome pathway enrichment analysis. The red box indicated that the PI3K/AKT signaling pathway has a high enrichment factor, suggesting its potential role in LPS pre-EVs-mediated treatment of IBD. **(F)** Western blot validation results. ****$P < 0.0001$.

differences in protein expression patterns between the LPS pre-EVs group and the other treatment groups. Reactome pathway enrichment analysis (Figure 7E) showed that the differential proteins were predominantly enriched in biological processes related to metabolism and signal transduction, particularly the mesenchymal-epithelial transition factor-activated PI3K/AKT signaling pathway, which was significantly enriched in the LPS pre-EVs group. Western blot validation results (Figure 7F) further confirmed the differential expression of PI3K, p-PI3K, AKT, and p-AKT across the treatment groups. The relative expression levels of p-PI3K/PI3K and p-AKT/AKT were significantly higher in the LPS pre-EVs group compared to the other groups, suggesting that LPS pre-EVs may play a crucial role in the treatment of IBD in mice by activating the PI3K/AKT signaling pathway.

Discussion

In this study, we extracted P-EVs and LPS pre-EVs, and administered them via tail vein injection into a mouse model of colitis, respectively. With small animal live imaging, we also observed fluorescence in the lungs and spleens of mice, probably because the injected DiR-labelled EVs are distributed throughout the body through the blood circulation, and high blood flow organs such as the lungs and spleens can easily capture the EVs. In addition, these organs may be involved in the metabolic clearance of EVs or may absorb EVs due to the inflammatory response that affects the systemic immune system. Therefore, the discovery of EVs at these sites may be the result of a combination of their systemic distribution, the clearance function of the organs, and systemic inflammation.[15,19] Further experiments, such as tracking techniques using different markers or studying organ-specific receptor expression, are needed to better understand the distribution mechanism of EVs in different organs. The results demonstrated that LPS pre-EVs significantly improved inflammation-related indicators, such as reduced weight loss, improved DAI scores, and restoration of colon length, indicating strong anti-inflammatory effects. Compared to P-EVs, LPS pre-EVs showed more pronounced effects in mitigating weight loss and improving DAI scores, suggesting that LPS preconditioning may enhance the anti-inflammatory efficacy of EVs by modulating their bioactivity or targeting specificity. Previous studies have shown that MSCs co-cultured with inflammatory cytokines or small-molecule inflammatory agents exhibit significantly enhanced migration to injury sites, paracrine functions, and immunomodulatory capabilities.[31–34] EVs play a crucial role in these paracrine functions by delivering signaling molecules, regulating the microenvironment, and facilitating targeted communication between cells.[37,38] This study further confirmed that the preconditioning of PDLSCs using inflammatory factors could influence the therapeutic efficacy of EVs in IBD treatment by affecting their interaction with the host immune system.[16,39,40]

In the LPS pre-EVs group, the expression of the M2 macrophage marker Arg-1 in the intestinal tissue was significantly up-regulated, while the expression of the M1 macrophage marker iNOS was significantly lower, indicating that LPS pre-EVs may exert their anti-inflammatory effects by promoting the macrophages toward the anti-inflammatory M2 phenotype. In this study, the PI3K/AKT signaling pathway likely played a crucial role in the polarization of macrophages, promoting the secretion of anti-inflammatory cytokines like IL-10, which aids in controlling inflammation and facilitating tissue repair, thereby skewing intestinal macrophages toward the M2 phenotype.[41] However, the role of LPS pre-EVs in M1 polarization is more complex. Some in vitro studies have shown a tendency for macrophages to polarize toward the M1 phenotype, which contrasts with the findings of this study and previous research.[42,43] As for the possible causes for the phenomenon, the choice of preconditioning methods, the differences between in vivo and in vitro models, and different experimental conditions may be involved and influence functional signaling pathways in macrophages.[44] Moreover, LPS pre-EVs were shown to significantly enhance the expression of tight junction proteins in the intestinal epithelium and maintain the integrity of the epithelial barrier, thereby preventing the further spread of inflammation by strengthening barrier function.

The gut microbiota plays a critical role in the pathogenesis of IBD.[45,46] Through 16S rRNA gene sequencing analysis, this study revealed that LPS pre-EVs significantly altered the gut microbiota composition in IBD mice, notably increasing the abundance of beneficial bacteria such as *Clostridia_UCG-014*, while suppressing the overgrowth of potential pathogens like *Streptococcus*, demonstrating that LPS pre-EVs may exert their anti-inflammatory effects indirectly by modulating the balance of the gut microbiota. Future research should further investigate the mechanisms of interaction between EVs and the gut microbiota and explore whether combining EVs with probiotics or specific dietary interventions could enhance their therapeutic effects.[47]

As a crucial signaling pathway in regulating cell proliferation, survival, and inflammatory responses, PI3K/AKT was found to be activated in this study through which LPS pre-EVs significantly influenced protein expression related to

inflammation and tissue repair in the mouse gut. In this study, we observed significant activation of the PI3K/AKT pathway, with distinct biological functions displayed at key phosphorylation sites on AKT. Thr308 and Ser473 are two major phosphorylation sites, each with unique physiological roles. Phosphorylation at Thr308, primarily mediated by PDK1, is essential for the initial activation of AKT's kinase activity, which regulates cell proliferation and metabolic processes. In contrast, phosphorylation at Ser473, generally controlled by mTORC2, is crucial for the full activation of AKT, supporting cell survival and inhibiting apoptosis. Here, we assessed AKT activation by specifically examining phosphorylation at Ser473 to understand the precise signaling changes. This differential phosphorylation enables AKT to regulate a range of functions, including inflammatory response modulation and tissue repair, both critical in alleviating colitis and restoring the intestinal barrier. Based on our findings, LPS-pretreated PDLSC-derived EVs may exert enhanced anti-inflammatory and regenerative effects by specifically activating AKT at Ser473. Previous studies have also demonstrated the significance of different signaling pathways responsible for the therapeutic effects of EVs in IBD.[14,25,48] Exosomes from hypoxia-preconditioned hair follicle MSCs may alleviate ulcerative colitis by inhibiting the PI3K/AKT/mTOR signaling pathway through miR-214-3p, maintaining mitochondrial dynamics stability, reducing mitochondrial dysfunction, and enhancing mitophagy.[49] Additionally, exosomes derived from human umbilical cord MSCs has been shown to accelerate intestinal stem cell and epithelial regeneration through the activation of the Wnt signaling pathway, thereby promoting mucosal healing in experimental colitis.[14] Moreover, bone marrow MSCs-derived EVs containing miR-539-5p were found to alleviate pyroptosis in IBD by inhibiting the NLRP3/caspase-1 signaling pathway.[25] Similarly, exosomes derived from umbilical cord MSCs were shown to reduce colitis by regulating macrophage pyroptosis via the miR-378a-5p/NLRP3 axis.[48] These studies collectively highlight the important roles of exosomes in the treatment of IBD through various signaling pathways and molecular mechanisms. Future in-depth studies could explore how LPS pre-EVs regulate gut proteins and their functions, and evaluate the involvement of additional key signaling pathways in exosome-mediated IBD therapy.

The DSS-induced mouse model primarily reflects the pathological characteristics of acute colitis, which may not fully represent the pathophysiological mechanisms of other types of IBD, such as chronic colitis.[50,51] Therefore, IBD models induced by other methods should be used to examine the effects of LPS pre-EVs. While this study explored the role of LPS pre-EVs in regulating intestinal macrophage polarization, gut barrier function, gut microbiota composition, and intestinal protein expression, the specific components within the EVs, such as miRNAs, proteins, or lipids, that may contribute to these regulatory processes remain to be elucidated.[15] Further studies are needed to investigate the molecular mechanisms by which these specific components of the EVs influence the pathways.

Conclusion

Collectively, our study demonstrated that LPS pre-EVs is capable of exhibiting immunomodulatory and anti-inflammatory functions, maintaining intestinal epithelial barrier function, and regulating gut microbiota composition in vivo, and thus is a promising and effective method in experimental IBD. These findings not only provide new insights into the immunomodulatory potential of dental stem cell-derived EVs but also offer new avenues for the future clinical treatment of IBD.

Data Sharing Statement

The data will be available from the corresponding authors.

Acknowledgments

Graphical Abstract was created by using Figdraw (www.figdraw.com).

Author Contributions

All authors made a significant contribution to the work reported, whether that is in the conception, study design, execution, acquisition of data, analysis and interpretation, or in all these areas; took part in drafting, revising or critically reviewing the article; gave final approval of the version to be published; have agreed on the journal to which the article has been submitted; and agree to be accountable for all aspects of the work.

Funding

This work was supported by grants from the National Natural Science Foundation of China (Nos.82071080 and 82470951 to Fulan Wei, No.81570945 to Gang Ding), the Natural Science Foundation of Shandong Province (No. ZR2024MH147 to Gang Ding), and Weifang Kite Capital Scholars Program (No. ydxz2023002 to Gang Ding).

Disclosure

The authors report no conflicts of interest in this work.

References

1. Li J, Simmons AJ, Hawkins CV, et al. Identification and multimodal characterization of a specialized epithelial cell type associated with Crohn's disease. *Nat Commun*. 2024;15(1):7204. doi:10.1038/s41467-024-51580-7
2. Rosen MJ, Dhawan A, Saeed SA. Inflammatory bowel disease in children and adolescents. *JAMA Pediatr*. 2015;169(11):1053–1060. doi:10.1001/jamapediatrics.2015.1982
3. Agrawal M, Allin KH, Petralia F, Colombel JF, Jess T. Multiomics to elucidate inflammatory bowel disease risk factors and pathways. *Nat Rev Gastroenterol Hepatol*. 2022;19(6):399–409. doi:10.1038/s41575-022-00593-y
4. Gilliland A, Chan JJ, De Wolfe TJ, Yang H, Vallance BA. Pathobionts in inflammatory bowel disease: origins, underlying mechanisms, and implications for clinical care. *Gastroenterology*. 2024;166(1):44–58. doi:10.1053/j.gastro.2023.09.019
5. Bisgaard TH, Allin KH, Keefer L, Ananthakrishnan AN, Jess T. Depression and anxiety in inflammatory bowel disease: epidemiology, mechanisms and treatment. *Nat Rev Gastroenterol Hepatol*. 2022;19(11):717–726. doi:10.1038/s41575-022-00634-6
6. Lerchova T, Mårild K, Ludvigsson J. Population-based birth cohort studies, a powerful design to identify childhood environmental risk factors for inflammatory bowel disease. *United Eur Gastroenterol J*. 2024;12(1):157–158. doi:10.1002/ueg2.12522
7. Liu D, Saikam V, Skrada KA, Merlin D, Iyer SS. Inflammatory bowel disease biomarkers. *Med Res Rev*. 2022;42(5):1856–1887. doi:10.1002/med.21893
8. Kaplan GG, Windsor JW. The four epidemiological stages in the global evolution of inflammatory bowel disease. *Nat Rev Gastroenterol Hepatol*. 2021;18(1):56–66. doi:10.1038/s41575-020-00360-x
9. Park J, Cheon JH. Incidence and prevalence of inflammatory bowel disease across Asia. *Yonsei Med J*. 2021;62(2):99–108. doi:10.3349/ymj.2021.62.2.99
10. Xu L, He B, Sun Y, et al. Incidence of inflammatory bowel disease in urban China: a nationwide population-based study. *Clin Gastroenterol Hepatol*. 2023;21(13):3379–3386.e29. doi:10.1016/j.cgh.2023.08.013
11. Okamoto R, Mizutani T, Shimizu H. Development and application of regenerative medicine in inflammatory bowel disease. *Digestion*. 2023;104(1):24–29. doi:10.1159/000527423
12. Plevris N, Lees CW. Disease Monitoring in inflammatory bowel disease: evolving principles and possibilities. *Gastroenterology*. 2022;162(5):1456–1475.e1. doi:10.1053/j.gastro.2022.01.024
13. Lee JH, Lötvall J, Cho BS. The anti-inflammatory effects of adipose tissue mesenchymal stem cell exosomes in a mouse model of inflammatory bowel disease. *Int J Mol Sci*. 2023;24(23):16877. doi:10.3390/ijms242316877
14. Liang X, Li C, Song J, et al. HucMSC-Exo promote mucosal healing in experimental colitis by accelerating intestinal stem cells and epithelium regeneration via Wnt signaling pathway. *Int J Nanomed*. 2023;18:2799–2818. doi:10.2147/ijn.S402179
15. Wang G, Yuan J, Cai X, et al. HucMSC-exosomes carrying miR-326 inhibit neddylation to relieve inflammatory bowel disease in mice. *Clin Transl Med*. 2020;10(2):e113. doi:10.1002/ctm2.113
16. Yang R, Huang H, Cui S, Zhou Y, Zhang T, Zhou Y. IFN-γ promoted exosomes from mesenchymal stem cells to attenuate colitis via miR-125a and miR-125b. *Cell Death Dis*. 2020;11(7):603. doi:10.1038/s41419-020-02788-0
17. Li X, Jiang Y, Liu X, et al. Mesenchymal stem cell-derived apoptotic bodies alleviate alveolar bone destruction by regulating osteoclast differentiation and function. *Int J Oral Sci*. 2023;15(1):51. doi:10.1038/s41368-023-00255-y
18. Yang S, Liang X, Song J, et al. A novel therapeutic approach for inflammatory bowel disease by exosomes derived from human umbilical cord mesenchymal stem cells to repair intestinal barrier via TSG-6. *Stem Cell Res Ther*. 2021;12(1):315. doi:10.1186/s13287-021-02404-8
19. Yan Y, Li K, Jiang J, et al. Perinatal tissue-derived exosomes ameliorate colitis in mice by regulating the Foxp3 + Treg cells and gut microbiota. *Stem Cell Res Ther*. 2023;14(1):43. doi:10.1186/s13287-023-03263-1
20. Tian J, Chen W, Xiong Y, et al. Small extracellular vesicles derived from hypoxic preconditioned dental pulp stem cells ameliorate inflammatory osteolysis by modulating macrophage polarization and osteoclastogenesis. *Bioact Mater*. 2022;22:326–342. doi:10.1016/j.bioactmat.2022.10.001
21. Kalluri R, LeBleu VS. The biology, function, and biomedical applications of exosomes. *Science*. 2020;367(6478):eaau6977. doi:10.1126/science.aau6977
22. van Niel G, D'Angelo G, Raposo G. Shedding light on the cell biology of extracellular vesicles. *Nat Rev Mol Cell Biol*. 2018;19(4):213–228. doi:10.1038/nrm.2017.125
23. Keshtkar S, Azarpira N, Ghahremani M. Mesenchymal stem cell-derived extracellular vesicles: novel frontiers in regenerative medicine. *Stem Cell Res Ther*. 2018;9(1):63. doi:10.1186/s13287-018-0791-7
24. Xia L, Zhang C, Lv N, et al. AdMSC-derived exosomes alleviate acute lung injury via transferring mitochondrial component to improve homeostasis of alveolar macrophages. *Theranostics*. 2022;12(6):2928–2947. doi:10.7150/thno.69533
25. Wang D, Xue H, Tan J, et al. Bone marrow mesenchymal stem cells-derived exosomes containing miR-539-5p inhibit pyroptosis through NLRP3/caspase-1 signalling to alleviate inflammatory bowel disease. *Inflamm Res*. 2022;71(7–8):833–846. doi:10.1007/s00011-022-01577-z
26. Mao F, Wu Y, Tang X, et al. Exosomes derived from human umbilical cord mesenchymal stem cells relieve inflammatory bowel disease in mice. *Biomed Res Int*. 2017(2017):5356760. doi:10.1155/2017/5356760

27. Maeda H, Tomokiyo A, Fujii S, Wada N, Akamine A. Promise of periodontal ligament stem cells in regeneration of periodontium. *Stem Cell Res Ther*. 2011;2(4):33. doi:10.1186/scrt74
28. Liu J, Chen B, Bao J, Zhang Y, Lei L, Yan F. Macrophage polarization in periodontal ligament stem cells enhanced periodontal regeneration. *Stem Cell Res Ther*. 2019;10(1):320. doi:10.1186/s13287-019-1409-4
29. Gan L, Liu Y, Cui D, Pan Y, Zheng L, Wan M. Dental tissue-derived human mesenchymal stem cells and their potential in therapeutic application. *Stem Cells Int*. 2020(2020):8864572. doi:10.1155/2020/8864572
30. Calabrese E. Human periodontal ligament stem cells and hormesis: enhancing cell renewal and cell differentiation. *Pharmacol Res*. 2021;173:105914. doi:10.1016/j.phrs.2021.105914
31. Ti D, Hao H, Tong C, et al. LPS-preconditioned mesenchymal stromal cells modify macrophage polarization for resolution of chronic inflammation via exosome-shuttled let-7b. *J Transl Med*. 2015;13:308. doi:10.1186/s12967-015-0642-6
32. Cabezas J, Rojas D, Wong Y, et al. In vitro preconditioning of equine adipose mesenchymal stem cells with prostaglandin E(2), substance P and their combination changes the cellular protein secretomics and improves their immunomodulatory competence without compromising stemness. *Vet Immunol Immu*. 2020;228:110100. doi:10.1016/j.vetimm.2020.110100
33. Liu K, Cai GL, Zhuang Z, et al. Interleukin-1β-treated mesenchymal stem cells inhibit inflammation in hippocampal astrocytes through exosome-activated Nrf-2 signaling. *Int J Nanomed*. 2021;16:1423–1434. doi:10.2147/ijn.S289914
34. Sanap A, Kheur S, Kharat A, Bhonde R. Ascorbic acid and IFNγ preconditioning enhance the potency of human mesenchymal stem cells to ameliorate LPS induced cytokine storm. *Int Immunopharmacol*. 2023;122:110643. doi:10.1016/j.intimp.2023.110643
35. Zhou Y, Zheng L, Zhou X, Li J, Xu X. Dental mesenchymal stem cells in inflamed microenvironment: potentials and challenges for regeneration. *Curr Stem Cell Res Ther*. 2015;10(5):412–421. doi:10.2174/1574888X10666150312102324
36. Xu Y, Zhu J, Feng B, et al. Immunosuppressive effect of mesenchymal stem cells on lung and gut CD8(+) T cells in lipopolysaccharide-induced acute lung injury in mice. *Cell Prolif*. 2021;54(5):e13028. doi:10.1111/cpr.13028
37. Wang C, Jiang C, Yang Y, et al. Therapeutic potential of HUC-MSC-exos primed with IFN-γ against LPS-induced acute lung injury. *Iran J Basic Med Sci*. 2024;27(3):375–382. doi:10.22038/ijbms.2023.74372.16156
38. Duan A, Shen K, Li B, et al. Extracellular vesicles derived from LPS-preconditioned human synovial mesenchymal stem cells inhibit extracellular matrix degradation and prevent osteoarthritis of the knee in a mouse model. *Stem Cell Res Ther*. 2021;12(1):427. doi:10.1186/s13287-021-02507-2
39. Ge W, Luo S, Zhang K, Liu L, Zhou Z, Liu Y. Role of histone deacetylase 9 in human periodontal ligament stem cells autophagy in a tumour necrosis factor α-induced inflammatory environment. *Tissue Cell*. 2023;82:102113. doi:10.1016/j.tice.2023.102113
40. Wang S, Wu R, Chen Q, Liu T, Li L. Li L.Exosomes derived from TNF-α-treated bone marrow mesenchymal stem cells ameliorate myocardial infarction injury in mice. *Organogenesis*. 2024;20(1):2356341. doi:10.1080/15476278.2024.2356341.
41. Zhang P, Wu P, Khan UZ, et al. Exosomes derived from LPS-preconditioned bone marrow-derived MSC modulate macrophage plasticity to promote allograft survival via the NF-κB/NLRP3 signaling pathway. *J Nanobiotechnology*. 2023;21(1):332. doi:10.1186/s12951-023-02087-8
42. Kang H, Lee MJ, Park SJ, Lee MS. Lipopolysaccharide-preconditioned periodontal ligament stem cells induce M1 polarization of macrophages through extracellular vesicles. *Int J Mol Sci*. 2018;19(12):3843. doi:10.3390/ijms19123843
43. Cui S, Zhang Z, Cheng C, et al. Small extracellular vesicles from periodontal ligament stem cells primed by lipopolysaccharide regulate macrophage M1 polarization via miR-433-3p targeting TLR2/TLR4/NF-κB. *Inflammation*. 2023;46(5):1849–1858. doi:10.1007/s10753-023-01845-y
44. Liu X, Tan GR, Yu M, et al. The effect of tumour necrosis factor-α on periodontal ligament stem cell differentiation and the related signaling pathways. *Curr Stem Cell Res Ther*. 2016;11(7):593–602. doi:10.2174/1574888X11666160429122858
45. Sittipo P, Lobionda S, Lee YK, Maynard CL. Intestinal microbiota and the immune system in metabolic diseases. *J Microbiol*. 2018;56(3):154–162. doi:10.1007/s12275-018-7548-y
46. Milani C, Duranti S, Bottacini F, et al. The first microbial colonizers of the human gut: composition, activities, and health implications of the infant gut microbiota. *Microbiol Mol Biol Rev*. 2017;81(4):e00036. doi:10.1128/MMBR.00036-17
47. Kayama H, Okumura R, Takeda K. Interaction between the microbiota, epithelia, and immune cells in the intestine. *Annu Rev Immunol*. 2020;38(1):23–48. doi:10.1146/annurev-immunol-070119-115104
48. Cai X, Zhang ZY, Yuan JT, et al. hucMSC-derived exosomes attenuate colitis by regulating macrophage pyroptosis via the miR-378a-5p/NLRP3 axis. *Stem Cell Res Ther*. 2021;12(1):416. doi:10.1186/s13287-021-02492-6
49. Li N, Zhao L, Geng X, et al. Stimulation by exosomes from hypoxia- preconditioned hair follicle mesenchymal stem cells facilitates mitophagy by inhibiting the PI3K/AKT/mTOR signaling pathway to alleviate ulcerative colitis. *Theranostics*. 2024;14(11):4278–4296. doi:10.7150/thno.96038
50. Schepelmann M, Kupper N, Gushchina V, et al. AOM/DSS induced colitis-associated colorectal cancer in 14-month-old female Balb/C and C57/Bl6 mice-a pilot study. *Int J Mol Sci*. 2022;23(9):5278. doi:10.3390/ijms23095278
51. Chen Y, Zhang P, Chen W, Chen G. Ferroptosis mediated DSS-induced ulcerative colitis associated with Nrf2/HO-1 signaling pathway. *Immunol Lett*. 2020;225:9–15. doi:10.1016/j.imlet.2020.06.005